THE EUROPEAN
PHYSICAL JOURNAL PLUS

Regular Article

Study of (n, 2n) reaction cross sections for ^{107}Ag within the energy range of 9–22 MeV

Rakesh Chauhan[1,a] , **R. K. Singh**[1], **N. L. Singh**[1,b], **Mayur Mehta**[2],
Rajnikant Makwana[1], **S. V. Suryanarayana**[3], **S. Mukherjee**[1], **B. K. Nayak**[4], **H. Naik**[4],
J. Varmuza[5], **K. Katovsky**[5]

[1] Department of Physics, Faculty of Science, The M. S. University of Baroda, Vadodara 390002, India
[2] Institute for Plasma Research, Gandhinagar 382428, India
[3] Nuclear Physics Division, Bhabha Atomic Research Centre, Mumbai, India
[4] Radiochemistry Division, Bhabha Atomic Research Centre, Mumbai, India
[5] Department of Electrical Power Engineering, Brno University of Technology, Brno 61600, Czech Republic

Abstract The ^{107}Ag(n, 2n)^{106m}Ag reaction cross sections at the neutron energies of
10.50 ± 0.68, 13.52 ± 0.67, 16.86 ± 0.58 and 19.86 ± 0.59 MeV were measured by using
the off-line γ-ray spectroscopy and activation analysis techniques. The ^{7}Li(p, n) reaction
was used to produce the high-energy quasi-monoenergetic neutrons with the proton beam
from the 14UD BARC-TIFR Pelletron facilities at Mumbai, India. The neutron flux was mon-
itored using the standard ^{27}Al(n, α)^{24}Na monitor reaction. The detailed uncertainties analysis
in the measured cross sections was performed using the covariance analysis. The cross sec-
tions were also theoretically calculated using TALYS-1.9 code from 10 to 25 MeV energies.
The measured cross-sections data are compared with the evaluated data from TENDL-2019,
JENDL-4.0 and ENDF/B-VIII.0 libraries as well as with the existing experimental data
available in EXFOR compilation. Our data show good agreement with some of the previous
experimental data and with the theoretical values calculated with TALYS-1.9 code. Present
work will provide better description of level density models and pre-equilibrium process.

1 Introduction

Studies of the neutron-induced reactions are of immense interest in reactor applications.
Nuclear reactor consists of structural materials, control rods, fuel and shielding materials,
etc. Therefore, when neutrons originated from fusion or fission reaction interact with these
materials, they change mechanical and physical properties of the materials. It is necessary to
have cross-section data for these materials at all possible neutron energies. Threshold reac-
tions including (n, n′) and (n, 2n) have been used extensively for determining the differential
flux (dΦ/dE) from neutron sources by foil activation techniques. The cross sections of (n, xn)
reactions are necessary for activation detectors which are used to probe energy components

of a neutron fluence. An example of such a detector is rhodium, which is monoisotopic [1]. The measured experimental and theoretical cross-sections data show large discrepancies at higher neutron energies. Compound nucleus (CN), direct and pre-equilibrium reaction channels play important role at neutron energies up to 20 MeV. Therefore, measured cross sections with better accuracy are needed for understanding these reactions channels. Recently, several articles on nuclear reactions at moderate excitation energies have been concerned with the emission of particles before the nucleus reaches statistical equilibrium [2].

This paper reports experimental $(n, 2n)$ excitation functions of silver nuclei for neutron energies up to 20 MeV. In an attempt to understand the reaction mechanism, the data have been compared to a model, which permits pre-equilibrium and statistical modes of decay. These cross-section data can be useful for developing theoretical model and to explain reaction mechanism. Silver is an important metal used in control rod in fission nuclear reactors. Several isotopes of silver are also formed as fission products in reactor. Hence, the neutron-induced reaction cross-sections data of Ag isotopes are important for nuclear applications. The $(n, 2n)$ reactions of the two naturally occurring silver isotopes are potentially useful for the dosimetry of short pulses of d + T neutrons, the cross sections being fairly high and the half-lives of the induced activities reasonably short [3, 4].

In the present work, the $(n, 2n)$ reaction cross sections for ^{107}Ag target were measured at 10.5, 13.52, 16.86 and 19.82 MeV neutron energies relative to the standard ^{27}Al$(n, \alpha)^{24}$Na monitor reaction. The present experimental results were compared with the data available in EXFOR [5] literature database and evaluated data from ENDF/B-VIII.0 [6], JENDL-4.0 [7] and TENDL-2019 [8] libraries. The nuclear reaction code TALYS-1.9 [9] was used for the theoretical calculation of reaction cross section by using different level density and pre-equilibrium models. A detailed analysis of the uncertainty in the measured cross section was performed using the covariance analysis.

2 Experimental set-up

The irradiation of the samples was done at the 14UD BARC-TIFR Pelletron Linac accelerator facility, Mumbai, India. The natural Ag sample in the form of pallet of area 1.131 cm^2 and thickness 0.041 cm was taken for the irradiation. Natural silver sample contains two isotopes of silver, namely Ag-107 and Ag-109. The threshold for ^{109}Ag$(n,4n)$ reaction is 26.23 MeV which is higher than the energies of neutrons used here to study ^{107}Ag$(n,2n)^{106m}$Ag reaction. So ^{109}Ag$(n,4n)^{106m}$Ag reaction channel does not affect our said reaction cross section for the neutron energy range of 10 to 20 MeV. ^{7}Li (p, n) ^{7}Be nuclear reaction was used for the production of the quasi-monoenergetic neutrons. The proton beam with specific energy was incident on natural lithium (Li) foil of thickness 7.8 mg/cm^2, which is sandwiched between the two tantalum (Ta) foils of different thickness. The front tantalum foil of thickness 3.2 mg/cm^2 which is facing the proton beam was used to protect Li foil from the damage due to direct exposure. The back tantalum foil of thickness 0.1 mm was used to stop the proton beam. The degradation of the proton energy in Li foil according to SRIM [10] calculation is 136.61–210.18 keV, which is small in comparison with the energy of the incident proton. The samples were placed at a distance of 2.1 cm at zero degree with respect to proton beam. The schematic experimental set-up for the irradiation of samples is given in Fig. 1. The samples used for neutron irradiation were wrapped in the 0.025 mm thick aluminium foil to prevent radioactive contamination from each other. After neutron irradiation, the samples were kept at a suitable distance from the window centre of the high-purity germanium (HPGe) detector. The reaction products from the activated samples emit γ-rays, and these γ-rays were counted
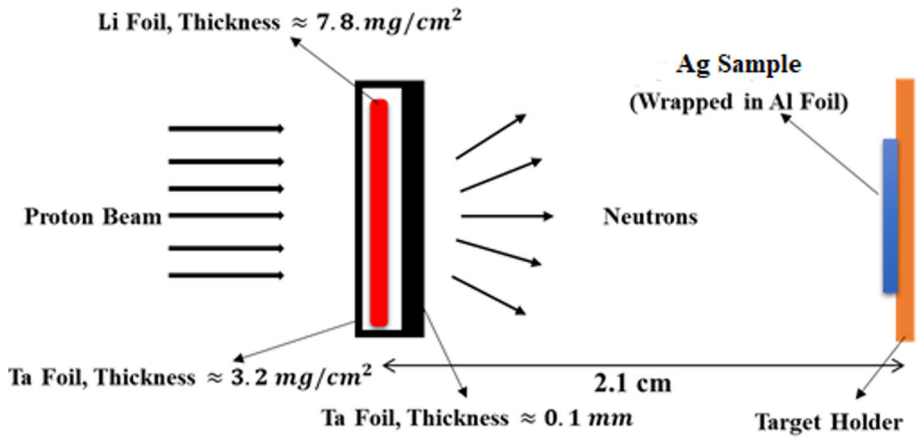
Li Foil, Thickness $\approx 7.8. mg/cm^2$

Ag Sample
(Wrapped in Al Foil)

Proton Beam

Neutrons

Ta Foil, Thickness $\approx 3.2\ mg/cm^2$

Ta Foil, Thickness $\approx 0.1\ mm$

2.1 cm

Target Holder

Fig. 1 A systematic arrangement of the experimental set-up used for neutron irradiation of the samples

with the precalibrated 80 cm^3 HPGe detector coupled to a PC-based 4096-channel analyser. The energy and absolute efficiency calibration of the HPGe detector was determined using a standard ^{152}Eu source and is shown in Fig. 2. The resolution of the HPGe detector was 1.8 keV full width at half maximum (FWHM) at 1332 keV γ-ray of ^{60}Co. A typical γ-ray spectra of reaction products measured using an HPGe detector is given in Figs. 3 and 4 for ^{107}Ag$(n,2n)^{106m}$Ag reaction and monitor reaction ^{27}Al$(n, \alpha)^{24}$Na, respectively. The 511 keV gamma is the most intense line from our reaction product but it is not used for our calculation here because of the reason that this gamma is also a product of reaction ^{107}Ag$(n,2n)^{106}$Ag with a different half-life of 23.96 min. Because the discrimination of counts for these two product isomers is not straightforward, we have chosen gamma rays with different energy, i.e. 1045.83 keV, for our analysis.

3 Data analysis

3.1 Neutron energy calculation

The reaction ^{nat}Li(p, n) was used for the production of fast quasi-monoenergetic neutrons. Natural lithium has two isotopes ^{6}Li and ^{7}Li with isotopic abundances of 7.42 and 92.58%, respectively. The ^{7}Li$(p, n)^7$Be reaction produces monoenergetic neutrons in between the proton energies of 1.9 and 2.4 MeV. However, above the proton energy of 2.4 MeV, the first excited state of ^{7}Be at 0.43 MeV produces the second group of neutrons (n_1) [11]. In ^{7}Li(p, n) reaction, for the proton energy below 5 MeV the zero-degree yield of these low energy neutrons is less than about 10% of the ground state yield. Thus, the usefulness of the monoenergetic neutron source is only slightly impaired. The three-body breakup reaction ^{7}Li$(p, n\ ^3$He$)^4$He takes place above 3.68 MeV, which contributes neutrons with primary neutron peak (n_0). The threshold for the reaction ^{7}Li$(p, n)^7$Be is 7.06 MeV. Above 7.06 MeV, the second excited of ^{7}Be also contributes to the primary neutron group. The primary neutron peak (n_0) has higher neutron energy and flux, and this peak is used to measure the ($n, 2n$) reaction cross section. The neutron spectrum was used for the neutron energy calculation based on the kinematic relation $\left(E_n = E_p - E_{th}\right)$ where E_p is the proton energy and E_{th}
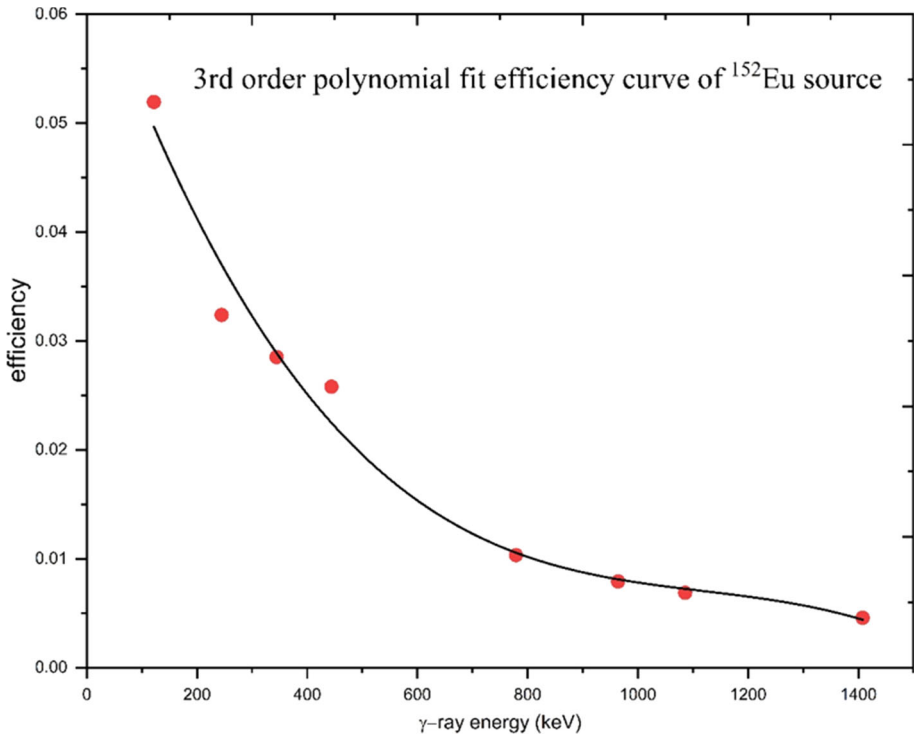
Fig. 2 Efficiency curve of HPGe detector with correction factor K_c for ^{152}Eu standard source

is the threshold energy of $^7Li(p, n)$ reaction. The effective average neutron energy of the primary neutron group from the neutron spectrum was calculated by using Eq. (1) as

$$
E_n = \frac{\int\limits_{E_{ps}}^{E_{max}} E_i \phi_i dE}{\int\limits_{E_{ps}}^{E_{max}} E_i dE}
\tag{1}
$$

where E_n = effective average neutron energy, E_{ps} = peak formation beginning for neutron energy in the generated spectrum, E_{max} = maximum neutron energy of the generated neutron spectrum, E_i = energy bin [14].

The uncertainty associated with this neutron energy was calculated from the width of monoenergetic part of the generated spectra. The neutron spectra based on the ^{7}Li(p, n) reaction for the proton energies 13, 16, and 19 and 22 MeV [15] are shown Fig. 5

3.2 Nuclear reaction cross-section measurement

The neutron activation cross sections were calculated by using the following relation,

$$
\langle \sigma_r \rangle = \langle \sigma_m \rangle . \frac{(\varepsilon . I_\gamma . Abu . Wt . f)_m}{(\varepsilon . I_\gamma . Abu . Wt . f)_r} . \frac{\left(C . \lambda . AM . \frac{CL}{LT}\right)_r}{\left(C . \lambda . AM . \frac{CL}{LT}\right)_m} . \prod_k \frac{C_{k_m}}{C_{k_r}}
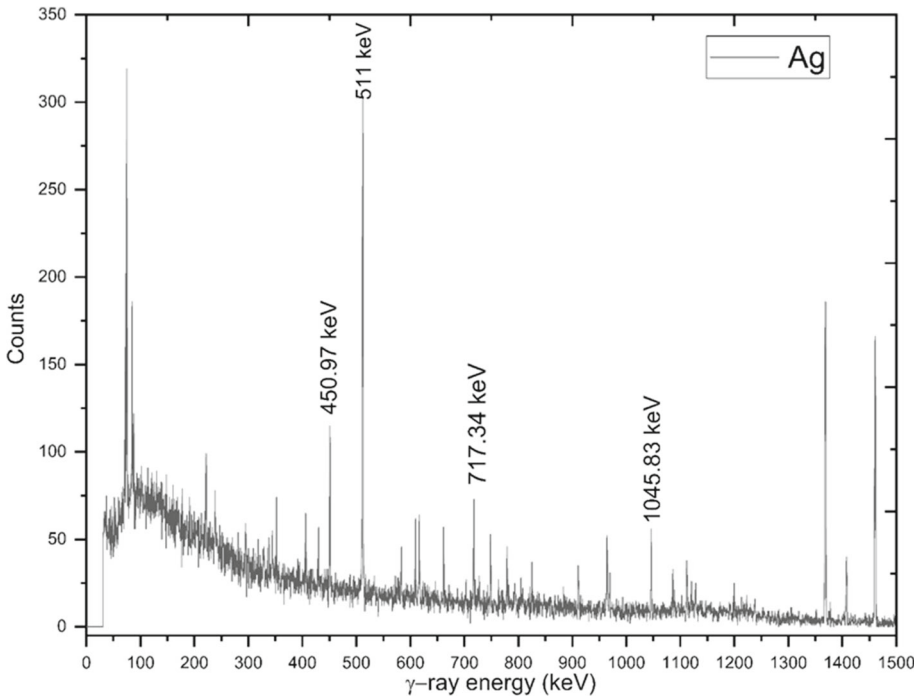\tag{2}
$$

Fig. 3 A gamma-ray spectrum of the decay of ^{106m}Ag to ^{106}Pd at an average neutron energy of 16.86 MeV. Previously known transitions of ^{106}Pd [11] are indicated

where r and m in subscript stand for reaction and monitor, σ_r and σ_m are sample and monitor reactions cross section, C is γ-ray photo-peak counts, λ is decay constant, ε is efficiency for characteristic γ-ray of radionuclide, I_r is γ-ray abundance, *Wt.* is weight, *Abu.* is isotopic abundance, *AM* is atomic mass, f is the time factor, CL and LT are the clock and live time, C_k is the correction factors due to the kth attributes, where k indicates the area, low energy neutron contribution and γ-ray self-attenuation factor, respectively. The following relation gives the time factor (f),

$$f = \left(1 - e^{-\lambda t_{irr}}\right).\left(1 - e^{-\lambda t_{count}}\right).e^{-\lambda t_{cool}}$$

where t_{irr} is the irradiation time, t_{cool} is the cooling time and t_{count} is the counting time. The cross sections for the monitor reaction ^{27}Al (n, α) ^{24}Na were calculated using the International Reactor Dosimetry and Fusion File (IRDFF-1.05) [16] data and by using a linear interpolation method at the nearest point energies. Spectroscopic and other data required for the calculation in Eq. (2) are as per Tables 1 and 2 for both cross section and monitor reactions. The calculated cross sections are 94.366$\pm$0.996, 125.456$\pm$0.525, 100.793$\pm$0.772 and 44.029$\pm$1.308 (mb) at the neutron energies of 10.51, 13.52, 16.86 and 19.89 MeV, respectively. The correction factor for γ–ray self-attenuation factor (Γ_{attn} for activated materials was calculated by the $\Gamma_{attn} = \left(\frac{1-e^{-\mu l}}{\mu l}\right)$ where l is the thickness of the materials and μ is the mass attenuation coefficient, which was taken from XMuDat ver.1.0.1 [17]. The following relation gives the correction for low energy neutron,
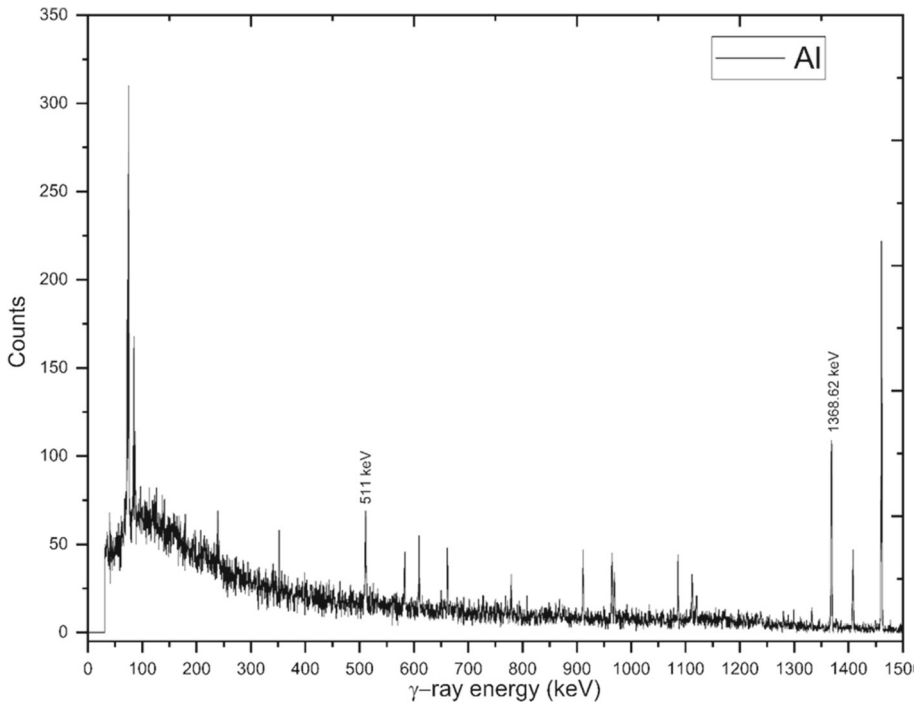
Fig. 4 A γ–ray spectrum of ^{24}Na decaying to ^{24}Mg from the ^{27}Al(n, α)^{24}Na monitor reaction at an average neutron energy of 16.86 MeV (1368.62 keV line)

$$\alpha_i = 1 + \frac{\beta_i}{\phi(E_{p_1})\sigma_i(E_{p_1})}, \beta_i = \phi(E_{p_2})\sigma_i(E_{p_2}) + \int_0^{E_{max}} \phi(E)\sigma_i(E)dE$$

where E_{p_1} and E_{p_2} are the primary and secondary neutron energy peaks in the neutron spectrum, $\phi(E)$ is the neutron flux and $\sigma_i(E)$ is the reaction cross sections. This cross sections $\sigma_i(E)$ for monitor and sample reaction were obtained from existing evaluated cross-section data ENDF/B-VIII.0 [6]. Following spectral indexing method, correction for low-energy neutrons is given in Ref. [18].

4 Covariance analysis

4.1 HPGe detector efficiency with covariance analysis

The following equation was used to calculate the efficiency of the HPGe detector,

$$\varepsilon = \frac{CK_c}{N_0 I_\gamma e^{-\lambda t}} \tag{3}$$

Here, ε is the efficiency of the corresponding $\gamma-$ rays, C is the counts under the photo-peak of γ-ray, N_0 is the activity of the standard ^{152}Eu source at an initial time, I_γ is the $\gamma-$ ray intensity, λ is the decay constant, and K_C is the correction factor for the coincidence
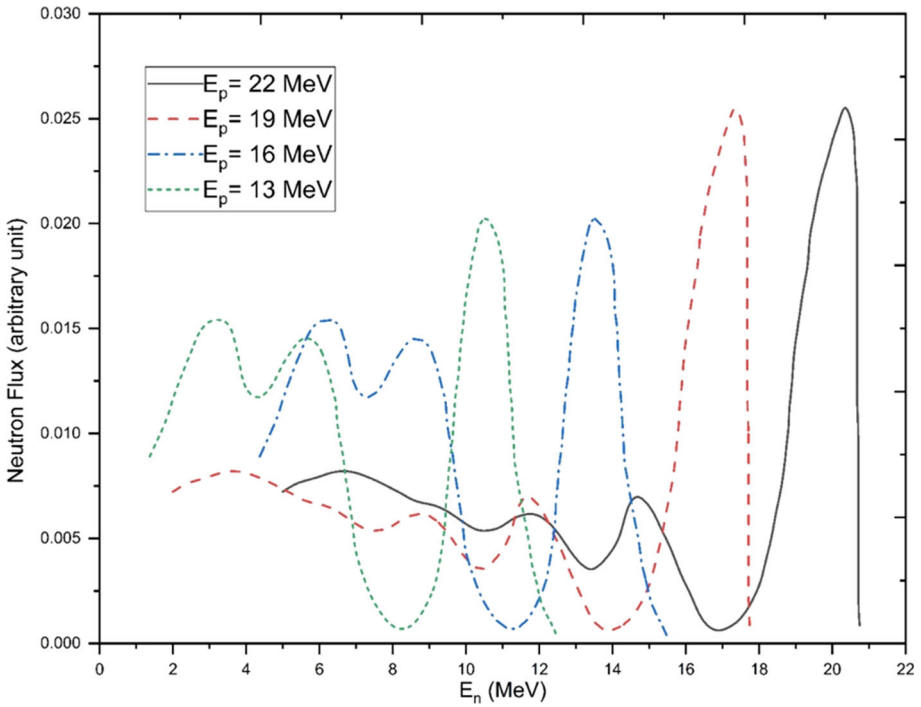
Fig. 5 Neutron energy spectra at 13, 16, 19 and 22 MeV protons energies from the ^{7}Li(p, n) reaction obtained from the Refs. data [12, 13]

summing effect in detecting $\gamma-$ rays. A Monte Carlo Simulation code EFFTRAN [19] was used for the calculation of correction factor K_C (see Table 3) by using HPGe coaxial detector structured data such as crystal hole cavity, end cup, mount cup, crystal material, dimension, absorber, window and calibration source information.

It is observed that the efficiency of the HPGe detector is the function of counts, decay constant, activity and $\gamma - ray$ intensity and uncertainty in these four variables propagates in the detector efficiency. Therefore, detector efficiency can be written as the function of only four attributes, such as I_γ, λ, C, $and N_0$. Partial uncertainties for the four attributes are listed in Table 3, which were used for the calculation of total uncertainties in the detector efficiency discussed below.

The total uncertainties due to four attributes in detector efficiency were calculated by using quadratic sum formula,

$$\left(\frac{\Delta\varepsilon_i}{\varepsilon_i}\right)^2 = \left(\frac{\Delta C_i}{C_i}\right)^2 + \left(\frac{\Delta I_{\gamma i}}{I_{\gamma i}}\right)^2 + \left(\frac{\Delta N_0}{N_0}\right)^2 + (t\Delta\lambda)^2 \tag{4}$$

Uncertainty in the decay constant is $\Delta\lambda = \dfrac{0.693\tau_{\frac{1}{2}}}{\tau^2_{\frac{1}{2}}}$

The covariance matrix for the HPGe detector efficiency was calculated from the given equation,

$$(V_\varepsilon)_{ij} = \sum_r e_{ir}S_{ijr}e_{jr}, \ 1 < i < 9, 1 < j < 9, 1 < r < 4 \tag{5}$$

Table 1 Spectroscopic data for the specified nuclear reaction product- ^{106m}Ag decaying to ^{106}Pd and for the monitor ^{27}Al(n,a) reaction product ^{24}Na decaying to ^{24}Mg

Isotopic Abundance (%)	Nuclear reaction	E_{th} (MeV)	Half-life ($\tau_{1/2}$)	Decay Mode	E_γ (keV)	I_γ (%)
51.84	^{107}Ag(n, 2n)^{106m}Ag	9.63	8.28 ± 0.02 days	β^+ (99.5%)	1045.83	29.62 ± 10
					717.34	28.9 ± 8
					450.97	28.2 ± 7
100	^{27}Al(n, α)^{24}Na	3.25	14.99 ± 0.12 h	β^- (100%)	1368.62	99.94 ± 4

Table 2 Proton energy, irradiation time and neutron flux of present experiment

Energy of proton (MeV)	13	16	19	22
Energy of neutron (MeV)	10.50 ± 0.68	13.52 ± 0.67	16.86 ± 0.55	19.89 ± 0.59
Irradiation time (sec)	37,200	28,080	21,900	18,900
Neutron flux (n/cm^2-sec)	7.26×10^5	1.27×10^6	2.78×10^6	3.36×10^6

Table 3 Partial uncertainties in the HPGe detector efficiency due to the different attributes

γ-ray energy (keV)	I_γ	C	N_0	$\tau_{1/2}$	K_c	Total uncertainty
121.7817	1.459×10^{-3}	1.597×10^{-4}	7.884×10^{-4}	2.329×10^{-3}	1.243	2.863×10^{-3}
244.6975	8.470×10^{-4}	2.002×10^{-4}	3.836×10^{-4}	1.133×10^{-3}	1.365	1.479×10^{-3}
344.2785	3.770×10^{-4}	8.923×10^{-5}	2.833×10^{-4}	8.369×10^{-4}	1.529	9.648×10^{-4}
443.965	4.392×10^{-4}	2.195×10^{-4}	2.008×10^{-4}	5.932×10^{-4}	1.213	7.958×10^{-4}
778.904	1.259×10^{-4}	6.950×10^{-5}	9.731×10^{-5}	2.874×10^{-4}	1.391	3.358×10^{-4}
964.079	1.024×10^{-4}	6.274×10^{-5}	8.082×10^{-5}	2.387×10^{-4}	1.421	2.792×10^{-4}
1085.869	1.276×10^{-4}	6.229×10^{-5}	7.038×10^{-5}	2.079×10^{-4}	1.121	2.614×10^{-4}
1408.006	4.653×10^{-5}	3.862×10^{-5}	4.620×10^{-5}	1.365×10^{-4}	1.371	1.563×10^{-4}

where V_ε is the covariance matrix, S_{ijr} is the $n \times n$ microcorrelation matrix between ith and jth observations due to the rth attributes and e_{ir} is the $n \times n$ diagonal matrix of partial uncertainties in ith observations due to the rth attributes. Similarly, e_{jr} is the $n \times n$ diagonal matrix of partial uncertainties in j^{th} observations due to the rth attributes. The calculated covariance matrix for HPGe detector efficiency is given in Table 4.

The γ-rays emitted by ^{106m}Ag, and ^{24}Na nuclei are different, and to estimate efficiencies for the corresponding γ-ray of ^{106m}Ag and ^{24}Na, a linear interpolation method was used in the calculation. An empirical relation as a model through interpolation uses the following linear parametric function,

$$ln(\varepsilon_i) = \sum_{k=1}^{m} p_k (ln[E_i])^{k-1}, \ 1 < i < 9, 1 < k < m \tag{6}$$

where ε_i is the efficiency for the corresponding γ-ray energy E_i and p_k is the fitting parameter.

The least-square condition states that the best estimate for P in the model is the one, which minimizes the Chi-square statistic given by,

Table 4 Covariance matrix for the HPGe detector efficiency

$$10^{-08} \begin{bmatrix} 820.1 \\ 294.1 & 218.8 \\ 217.2 & 105.6 & 93.08 \\ 153.9 & 74.91 & 55.33 & 63.32 \\ 74.61 & 36.29 & 26.81 & 19.01 & 11.27 \\ 61.96 & 30.14 & 22.26 & 15.78 & 7.646 & 7.793 \\ 53.96 & 26.25 & 19.39 & 13.74 & 6.659 & 5.531 & 6.833 \\ 43.55 & 21.19 & 15.65 & 11.09 & 5.375 & 4.464 & 3.888 & 6.247 \\ 35.43 & 17.23 & 12.73 & 9.025 & 4.372 & 3.631 & 3.163 & 2.552 & 2.418 \end{bmatrix}$$

Table 5 Covariance matrix for the ^{107}Ag(n, 2n)^{106m}Ag reaction cross sections at neutron energies of 10.5, 13.52, 16.86 and 19.81 MeV

$$10^{-08} \begin{bmatrix} 330.2 \\ 134.8 & 1355 \\ 107.3 & 213.5 & 855.2 \\ 94.81 & 188.6 & 150.1 & 418.9 \\ 175.6 & 106.1 & 84.48 & 74.73 & 2611 \\ 46.71 & 359.5 & 74.01 & 65.43 & 210.2 & 1859 \\ 44.21 & 88.01 & 231.1 & 61.94 & 199.1 & 174.2 & 888.9 \\ 3.352 & 6.673 & 5312 & 13.39 & 11.96 & 10.47 & 9.917 & 11.41 \end{bmatrix}$$

$$\chi^2_m = (Z - AP)' V_Z^{-1} (Z - AP)$$

From the least-square method, the best estimate of fitting parameter $\widehat{P}$ was calculated by the given relation,

$$\widehat{P} = \left(A^T V_z^{-1} A \right)^{-1} \left(A^T V_z^{-1} Z \right) \tag{7}$$

In the above equation, V_z can be calculated by equation $\frac{(V_\varepsilon)_{ij}}{\varepsilon_i \varepsilon_j}$, where V_ε is the covariance matrix, and ε_i is the efficiency. The best fit of the chosen model in the present work was obtained by considering six fitting parameters, and the model is given the best fit value for $m = 6$ and $i = 9$, with the goodness of fit $\chi^2 = 1.179$. We consider the following linear parametric model as the best model, which gives the value of fitting parameters ($p1 = -4.98363$, $p2 = -0.935804$, $p3 = -0.591703$, $p4 = -2.43244$, $p5 = -2.07165$, $p6 = -0.507021$).

From the above calculation, the covariance matrix and correlation matrix for the ^{107}Ag(n, 2n)^{106m}Ag reaction are given in Tables 5 and 6. The correlation matrix and measured efficiency for the characteristics γ-ray of ^{106m}Ag, and ^{24}Na are given in Table 7.

4.2 Uncertainty in the cross-section measurement

In covariance analysis ratio measure technique, a method was used for the activation cross-section calculation. In standard Eq. (2), the cross section of the sample was normalized to

Table 6 Correlation matrix for the ^{107}Ag(n, 2n)^{106m}Ag reaction cross sections for the neutron energies of 10.5, 13.52, 16.86 and 19.81 MeV

$$
\begin{bmatrix}
1.0 & & & & & & & \\
0.2016 & 1.0 & & & & & & \\
0.2019 & 0.1983 & 1.0 & & & & & \\
0.2549 & 0.2504 & 0.2507 & 1.0 & & & & \\
0.1891 & 0.0564 & 0.0565 & 0.0714 & 1.0 & & & \\
0.0596 & 0.2265 & 0.0586 & 0.0741 & 0.0954 & 1.0 & & \\
0.0815 & 0.0801 & 0.2651 & 0.1015 & 0.1306 & 0.1355 & 1.0 & \\
0.0546 & 0.0536 & 0.0538 & 0.1937 & 0.0693 & 0.0719 & 0.0985 & 1.0
\end{bmatrix}
$$

Table 7 Correlation matrix and measured efficiencies for the sample and monitor reactions

Nuclear reaction	γ-ray energy (MeV)	Efficiency	Correlation matrix
^{107}Ag(n, 2n)^{106m}Ag	0.45097		1.0
^{27}Al(n, α)^{24}Na	1.36862	$0.004372807 \pm 0.000163707$	0.6484 1.0
			0.9966 0.6683 1.0

monitor reaction cross section. We got the ratio of $\langle \sigma_r \rangle$ and $\langle \sigma_m \rangle$, i.e. the sample reaction cross section and monitor reaction cross section, which is given in Eq. (8),

$$
\langle \sigma_r \rangle = \langle \sigma_m \rangle . \frac{(\varepsilon . I_\gamma . Abu. Wt. f)_m}{(\varepsilon . I_\gamma . Abu. Wt. f)_r} . \frac{(C.\lambda.AM.\frac{CL}{LT})_r}{(C.\lambda.AM.\frac{CL}{LT})_m} . \prod_k \frac{C_{km}}{C_{kr}} \tag{8}
$$

The half-life, isotopic abundance, γ-ray abundance for sample and monitor reaction products with uncertainties are mentioned in Table 1. The nuclear data with uncertainties were taken from nuclear database [20, 21].

The complete covariance matrix for measured cross sections is given by the following relation,

$$
(V_{\sigma s})_{ij} = \sum_r e_{ir} S_{ijr} e_{jr} 1 \le i, j \le 14, 1 \le r \le 20 \tag{9}
$$

where S_{ijr} is the $n \times n$ microcorrelation matrix between ith and jth observations due to the rth attributes, e_{ir} is the partial uncertainty in ith observations due to the rth attributes and similarly for e_{jr}[22]. The uncertainties of different parameters contribute to the total uncertainty of the measured cross section. The source of uncertainty in the measured cross section and their values are as follows:

decay data (0.01–35%), area of γ-ray photo-peak (1–40%), efficiency of γ-detector (1.2–1.5%), corrections for self-absorption and γ-ray cascade summing (0.01–8.5%), reference cross sections used for neutron fluence determination (0.4–0.8%), sample mass (0.01–0.1%), isotopic abundance (0.01–7.5%). The contribution of uncertainties of other parameters is very small and can be neglected.

5 Theoretical calculation of reaction cross section with TALYS-1.9 code

A nuclear reaction modular code TALYS-1.9 [9] was used to understand the measured cross-section results. TALYS is a code for the simulation of nuclear reactions which simulates
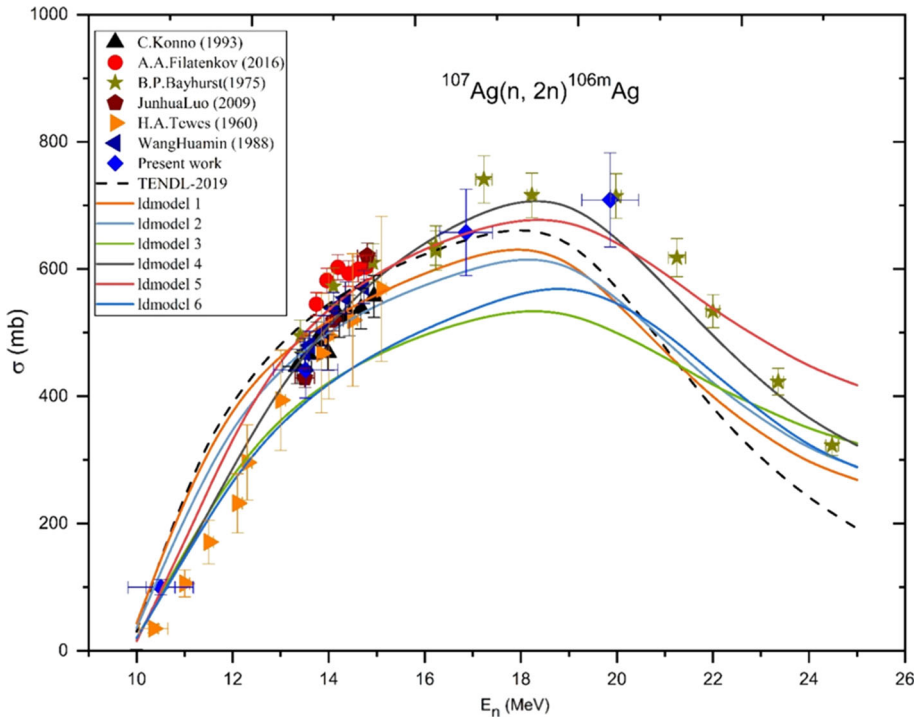
Fig. 6 Comparison of present work with the experimental data of EXFOR, theoretically calculated data from TALYS using different ldmodels and TENDL-2019 data

nuclear reactions that involve neutrons, γ-rays, protons, deuterons, tritons, helions, and alpha particles, in the 1 keV – 200 MeV energy range. This code considers the effect of level density parameters, compound, pre-equilibrium, and direct reaction mechanism as a function of incident particle energies. Koning and Delaroche proposed the optical model parameters by using a global potential [9]. In the present work, calculations were done with default parameters in TALYS except the change in level density (LD) model. The different level densities in the TALYS code (ldmodel 1–6) account for the constant temperature Fermi gas model (ldmodel 1) [23]; back-shifted Fermi gas model (ldmodel 2) [24]; generalized super-fluid model (ldmodel 3) [25, 26]; microscopic level densities from Goriely's and Hilaire's tables (ldmodel 4 and ldmodel 5) [27]; and microscopic level densities (ldmodel 6) (temperature-dependent HFB, Gogny force) [28], respectively. Theoretically calculated data are plotted in the graph for the comparison with the experimentally measured data. TENDL-2019 library data which are based on both default and adjusted parameters in the TALYS calculations and data from other sources, are also plotted in Fig. 6 for the comparison with the present work.

6 Results and discussion

In the present study, the ^{107}Ag(n,2n)^{106m}Ag reaction cross section has been measured at different neutron energies using the method of neutron activation. The off-line γ-ray spectroscopic technique was used for the estimation of activated nuclei produced in desired reaction

and monitor reaction ^{27}Al(n, α)^{24}Na for the measurement of neutron flux. The measured cross sections of ^{107}Ag(n,2n)^{106m}Ag reaction at the neutron energies of 10.50±0.68, 13.52±0.67, 16.86±0.55 and 19.89±0.59 MeV are 100.01±12, 441.432±44, 657.608±68 and 708.752±74 (mb), respectively.

The uncertainty in the cross-section measurement due to propagation of uncertainty in the quantities involved was calculated with the covariance analysis. The present work is plotted for comparison with the theoretical calculations as shown in Fig. 6. From the graph, it can be seen that the present work follows the trend of TALYS calculated data with ldmodel 4 and 5, and it overestimates the other ldmodels' calculations. The data are also in good agreement with the TENDL-2019 library of evaluated data. The present work is also in agreement with the experimental data taken from EXFOR data library reported by different authors. The present work will be helpful in the future reactor technology. It can be used for the betterment of the theoretical models for the simulation of nuclear reactions as well as for the improvement of the database of EXFOR for the neutron-induced reaction cross section of ^{107}Ag(n,2n)^{106m}Ag.

7 Summary and conclusions

In the present paper, the neutron-induced reaction cross sections of ^{107}Ag(n,2n)^{106m}Ag were measured at different neutron energies in the energy regime of the reactor applications. The Ag is an important reactor material used in control rod, and it is produced as fission fragments. The reaction cross-section measurement method is discussed. The neutrons are produced by the proton beam with energies 13.0, 16.0, 19.0, and 22.0 MeV targeted on natural lithium through ^{7}Li(p, n) reaction. For the selected energy range with this reaction, the generated neutrons are not purely monochromatic. Hence, the tailing corrections for low-energy neutrons and spectrum average cross sections were considered. The contribution of low energy neutrons has been removed to get the pure cross section from the reaction for the quasi-monoenergetic neutron. The correlation and uncertainties in the calculation of cross sections were estimated using the covariance analysis method. The measured cross sections are compared with evaluated data from TENDL-2019, JENDL-4.0 and ENDF/B-VIII.0 libraries as well as with existing experimental data available in EXFOR database. The nuclear level density models available in TALYS-1.9 code was used to predict cross section for the selected reactions.

References

1. B.P. Bayhurst, J.S. Gilmore, R.J. Prestwood, et al., Cross sections for (n, xn) reactions between 7.5 and 28 MeV. Phys. Rev. C 12(2) (1975). https://doi.org/10.1103/PhysRevC.12.451
2. H.M. Agrawal, K. Kailash Pandey, Surendra Babu et al., Neutron activation cross-sections at (14.6 ± 0.3) MeV. Ann. Nucl. Energy **35**, 1713–1719 (2008). https://doi.org/10.1016/j.anucene.2008.02.004
3. J. Luo, F. Tuo, X. Kong et al., Activation cross-section for reactions induced by 14 MeV neutrons on natural silver. Ann. Nucl. Energy **36**, 718–722 (2009). https://doi.org/10.1016/j.anucene.2009.02.009

4. N. Fotiades, M. Devlin, R.O. Nelson et al., Feeding of Rh and Ag isomers in fast-neutron-induced reactions. Phys. Rev. C **94**, 044608 (2016). https://doi.org/10.1103/PhysRevC.94.044608

5. Experimental Nuclear Reaction Data IAEA-EXFOR Database, https://www-nds.iaea.org/exfor/

6. D.A. Brown, M. Herman, A. Trkov et al., EDNF/B-VIII.0. Nucl. Data Sheets **148**, 1–142 (2018). https://doi.org/10.1016/j.nds.2018.02.001

7. K. Shibata, N. Iwamoto, S. Kunieda, F. Minato, O. Iwamoto "JENDL/AD-2017" "Activation Cross-section File for Decommissioning of LWRs" JAEA-Conf 2016–004, pp.47–52. https://wwwndc.jaea.go.jp/ftpnd/jendl/jendl-ad-2017.html

8. A.J. Koning, D. Rochman, M. Fleming et al., TENDL-2019. Nucl. Data Sheets **155**, 1–55 (2019). https://doi.org/10.1016/j.nds.2019.01.002

9. A.J. Koning, S. Hilaire, M.C. Duijvestijn, in *TALYS-1.0", Proceedings of the International Conference on Nuclear Data for Science and Technology*, April 22–27, 2007, Nice, France, ed. O. Bersillon, F. Gunsing, E. Bauge, R. Jacqmin, S. Leray. EDP Sciences (2008), pp. 211–214. https://doi.org/10.1051/ndata:07767

10. J.F. Ziegler, Nuclear instruments and methods in physics research section B: beam interactions with materials and atoms. Nucl. Instru. Methods B **219–220**, 1027 (2004). https://doi.org/10.1016/j.nimb.2004.01.208

11. D. De Frenne, A. Negret, Nuclear data sheets for A. Nucl. Data Sheets **109**, 943 (2008). https://doi.org/10.1016/j.nds.2008.03.002

12. C.H. Poppe, J.D. Anderson, J.C. Davis, S.M. Grimes, C. Wong, Cross sections for the ^{7}Li(p,n)^{7}Be reaction between 4.2 and 26 MeV. Phys. Rev. C **14**, 438 (1976). https://doi.org/10.1103/PhysRevC.14.438

13. M.W. Mcnaughton, N.S.P. King, F.P. Brady et al., Measurements of ^{7}Li(p,n) and ^{9}Be(p,n) cross sections at 15, 20 and 30 MeV. Nuclear Instruments And Methods **130**, 555–557 (1975). https://doi.org/10.1016/0029-554X(75)90057-9

14. Rajnikant Makwana, S. Mukherjee et al., Measurement of the cross section of the ^{186}W(n, γ)^{187}W, ^{182}W(n, p)^{182}Ta, ^{154}Gd(n, 2n)^{153}Gd, and ^{160}Gd(n, 2n)^{159}Gd reaction at neutron energies of 5 to 17 MeV. Phys. Rev. C **96**, 024608 (2017). https://doi.org/10.1103/PhysRevC.96.024608

15. S. Siddharth Parashari, H. Mukherjee, Naik, et al. Measurement of the ^{58}Ni(n, p)^{58}Co and ^{58}Ni(n, 2n)^{57}Ni reaction cross-sections for fast neutron energies up to 18 MeV. Eur. Phys. J. A **55**(4), 51 (2019). https://doi.org/10.1140/epja/i2019-12726-2.

16. E.M.Zsolnay, R. Capote, H.K. Nolthenius, and A. Trkov, Technical report INDC(NDS)-0616, IAEA, Vienna, 2012. https://www-nds.iaea.org/IRDFFv105/

17. Nowotny R (1998) XMuDat: photon attenuation data on PC. IAEA Report IAEA-NDS 195. https://www-nds.iaea.org/publications/iaea-nds-0195.htm

18. D.L. Smith, A.J.M. Plompen, V. Semkova, Corrections for low energy neutrons by spectral indexing, OECD, NEA, International Evaluation Co-operation, Volume-19, NEA/WPEC-19,ISBN 92–64–01070-X, 2005. https://www.oecd-nea.org/upload/docs/application/pdf/2019-12/volume19.pdf

19. T. Vidmar, EFFTRAN—A Monte Carlo efficiency transfer code for gamma-ray spectrometry. Nucl. Instrum. Methods Phys. Res., Sect. A **550**(3), 603–608 (2005). https://doi.org/10.1016/j.nima.2005.05.055

20. Jimin W, Xiaolong H, Nuclear data sheets for A=51. Nucl. Data Sheets **144**, 1–296 (2017). https://doi.org/10.1016/j.nds.2017.08.002

21. R.B. Firestone, Nucl. Data Sheets **108**, 2319 (2007). https://doi.org/10.1016/j.nds.2007.10.001

22. N. Otuka, B. Lalremruata, L.R.M. Punte et al., Uncertainty propagation in activation cross section measurements. Radiat. Phys. Chem. **140**, 502–510 (2017). https://doi.org/10.1016/j.radphyschem.2017.01.013

23. A. Gilbert, A.G.W. Cameron, A composite nuclear-level density formula with shell corrections. Can. J. Phys. **43**, 1446 (1965). https://doi.org/10.1139/p65-139

24. W. Dilg, W. Schantl, H. Vonach, M. Uhl, Level density parameters for the back-shifted fermi gas model in the mass range 40 < A < 250. Nucl. Phys. A **217**, 269 (1973). https://doi.org/10.1016/0375-9474(73)90196-6

25. A.V. Ignatyuk, K.K. Istekov, G.N. Smirenkin, Collective effects in level density, and the probability of fission. Sov. J. Nucl. Phys. **29**, 450 (1979). https://www.osti.gov/biblio/5176754

26. A.V. Ignatyuk, J.L. Weil, S. Raman, S. Kahane, Density of discrete levels in ^{116}Sn. Phys. Rev. C **47**, 1504 (1993). https://doi.org/10.1103/PhysRevC.47.1504

27. S. Goriely, S. Hilaire, A.J. Koning, Improved microscopic nuclear level densities within the Hartree-Fock-Bogoliubov plus combinatorial method. Phys. Rev. C **78**, 064307 (2008). https://doi.org/10.1103/PhysRevC.78.064307

28. S. Hilaire, M. Girod, S. Goriely, A.J. Koning, Temperature-dependent combinatorial level densities with the D1M Gogny force. Phys. Rev. C **86**, 064317 (2012). https://doi.org/10.1103/PhysRevC.86.064317